

The spatial frequency response and resolution limitations of pixelated mask spatial carrier based phase shifting interferometry

Brad Kimbrough, James Millerd

4D Technology Corporation, 3280 E. Hemisphere Loop, Suite 146, Tucson, AZ 85706

The spatial frequency response of the pixelated phase mask sensor has been investigated both theoretically and experimentally. Using the small phase step approximation, it is shown that the instrument transfer function can be approximated as the product of the system optical transfer function and the spatial carrier processing filter transfer function. To achieve optimum performance it is important that the bandwidth of the optical imaging system is adequate so that the limiting factor is the detector pixel width. Actual measurements on a commercial Fizeau interferometer agree very well with the theory, and demonstrate detector limited performance. The spatial resolution of the calculated phase map is algorithm dependent; however, both the 2x2 and 3x3 convolution algorithms result in a frequency response that is significantly more than what would be obtained by a simple parsing of the image. Therefore, a 1k x 1k sensor has a spatial frequency response that is approximately equal to the detector limited resolution of a 700 x 700 array with its frequency response extending to the full Nyquist limit of the 1k x 1k array.

Keywords: Interferometry, optical testing, spatial carrier

1. INTRODUCTION

This paper seeks to explore the phase resolution of the pixelated mask spatial carrier method.^{1,2,3} We start by providing a general overview of the spatial carrier phase shifting method which will allow us to make useful comparisons between the pixelated mask spatial carrier and the more typical linear spatial carrier methods. Next we discuss the concept of the instrument transfer function, ITF, and derive an expression for the ITF of the pixelated mask spatial carrier system under limiting conditions.

The expected performance of the pixelated mask spatial carrier system is verified in three different ways. First, a phase calculation is conducted on a simulated surface with a flat power spectrum and compared with the expected theoretical results. Next, modeling results are provided for an ITF calculation based on a small step height measurement and then compared with actual measured values. Finally, a smooth glass surface is measured and the power spectral density measurements are compared with theoretical results.

2. SPATIAL PHASE MEASUREMENT

Spatial phase measurement utilizes a single interferogram to extract phase information. In this technique, a spatially dependent carrier phase is added to the wavefront phase. A commonly used carrier phase is linear and produced by introducing a large tilt between the test and reference beams. The interference pattern produced may be represented as follows:

$$I(x, y) = I_{avg}(x, y)(1 + \nu \cos[\theta_w(x, y) + \phi_c(x, y)]) \quad (1)$$

where ν is the fringe visibility, $\theta_w(x, y)$ is the wavefront phase to be determined, and $\phi_c(x, y)$ is the carrier phase. A pixelated mask is another method of producing a carrier phase. Fundamentally the only difference between pixelated mask spatial carrier and other spatial carrier methods is the form of the carrier wavefront. For a null wavefront, the interferograms associated with both a linear and a pixelated carrier is shown in figure 1. The linear carrier phase is oriented at +45 deg. with a phase shift of 90 deg. between pixels in the x and y direction.

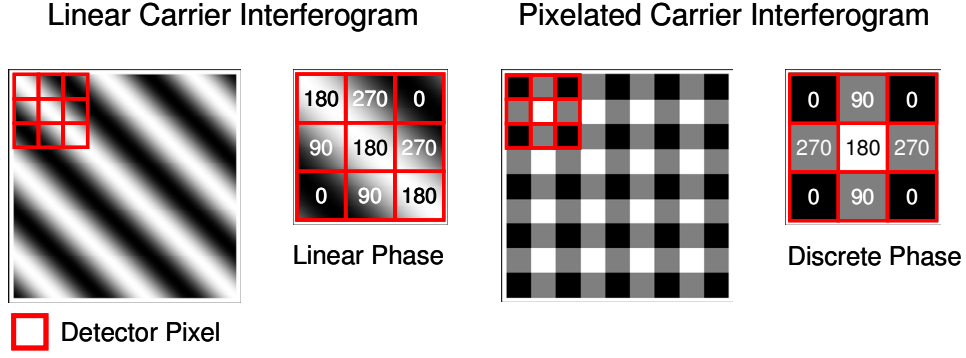


Figure 1. Null wavefront interferograms for a linear carrier and a pixelated carrier.

This particular linear carrier was chosen for comparison with the pixelated mask carrier since its performance most closely matches that of the pixelated mask. The linear carrier can be expressed analytically as shown in equation 2.

$$\phi_c(x, y) = \frac{\pi}{2}(x + y) \quad (2)$$

For the pixelated mask system, the carrier phase may be represented as two dimensional rectangular functions convolved with a two dimensional array of delta functions weighted with the necessary phase shift. This representation is shown in equation 3.

$$\phi_c(x, y) = \text{rect}[x, y] * \left(0 \text{comb}\left[\frac{x}{2}, \frac{y}{2}\right] + \frac{\pi}{2} \text{comb}\left[\frac{x-1}{2}, \frac{y-1}{2}\right] - \frac{\pi}{2} \text{comb}\left[\frac{x}{2}, \frac{y-1}{2}\right] + \pi \text{comb}\left[\frac{x-1}{2}, \frac{y}{2}\right] \right) \quad (3)$$

where $\text{rect}[x, y]$ is a two dimensional rectangle function representing the discrete size of each phase shift area, * represents the convolution operation, and the $\text{comb}[x, y]$ function represent a two dimensional grid of delta functions. Note that the $\text{comb}[x, y]$ function aligned with the zero phase shift regions has been explicitly included for clarification.

Using the linear carrier phase of equation 2, equation 1 may be expanded and written as follows:

$$I(x, y) = I_{avg}(x, y) + I_{avg}(x, y)v \text{Cos}[\theta_w(x, y)] \text{Cos}[\pi(x + y)] + I_{avg}(x, y)v \text{Sin}[\theta_w(x, y)] \text{Sin}[\pi(x + y)] \quad (4)$$

The interferogram intensity for the pixelated mask system is found by substituting the pixelated carrier phase of equation 5 into equation 1, and retaining only the fundamental carrier frequency terms. In this analysis, the finite extent of each phase shift region is ignored. With the exception of a slight change to fringe contrast, this simplification does not fundamentally alter the analysis since the fundamental carrier term is at the Nyquist frequency with all higher order terms aliasing back on top of it. The simplified result is given in equation 5.

$$I(x, y) = I_{avg}(x, y) + \frac{\sqrt{2}}{2} I_{avg}(x, y)v \text{Cos}[\theta'_w(x, y)] \text{Cos}[\pi x] + \frac{\sqrt{2}}{2} I_{avg}(x, y)v \text{Sin}[\theta'_w(x, y)] \text{Cos}[\pi y] \quad (5)$$

where $\theta'_w(x, y) = \theta_w(x, y) + \frac{\pi}{4}$.

Resolution limitations of the spatial carrier technique are most easily understood by examining the phase modulation and calculation process in the Fourier domain. The spectrum of the linear carrier interferogram is found by taking the Fourier transform of equation 4 with the results given in equation 6. Likewise the spectrum of the pixelated mask interferogram is given by the Fourier transform of equation 5 with the results given in equation 7.

$$\begin{aligned} \mathfrak{F}\{I(x, y)\} &= \mathfrak{F}\{I_{avg}(x, y)\} \\ &+ \mathfrak{F}\{I_{avg}(x, y)v\text{Cos}[\theta'_w(x, y)]\} * \frac{1}{2}(\delta[w_x - \frac{1}{4}, w_y - \frac{1}{4}] + \delta[w_x + \frac{1}{4}, w_y + \frac{1}{4}]) \\ &+ \mathfrak{F}\{I_{avg}(x, y)v\text{Sin}[\theta'_w(x, y)]\} * \frac{-i}{2}(\delta[w_x - \frac{1}{4}, w_y - \frac{1}{4}] - \delta[w_x + \frac{1}{4}, w_y + \frac{1}{4}]) \end{aligned} \quad (6)$$

$$\begin{aligned} \mathfrak{F}\{I(x, y)\} &= \mathfrak{F}\{I_{avg}(x, y)\} \\ &+ \frac{\sqrt{2}}{2} \mathfrak{F}\{I_{avg}(x, y)v\text{Cos}[\theta'_w(x, y)]\} * \frac{1}{2}(\delta[w_x - \frac{1}{2}] + \delta[w_x + \frac{1}{2}]) \\ &+ \frac{\sqrt{2}}{2} \mathfrak{F}\{I_{avg}(x, y)v\text{Sin}[\theta'_w(x, y)]\} * \frac{1}{2}(\delta[w_y - \frac{1}{2}] + \delta[w_y + \frac{1}{2}]) \end{aligned} \quad (7)$$

where $\delta[]$ is the Dirac delta function, (w_x, w_y) are the spatial frequency coordinates given in cycles/pixel and $*$ represents the convolution operation. The spectrums given in equations 6 and 7 are shown graphically in figure 2.

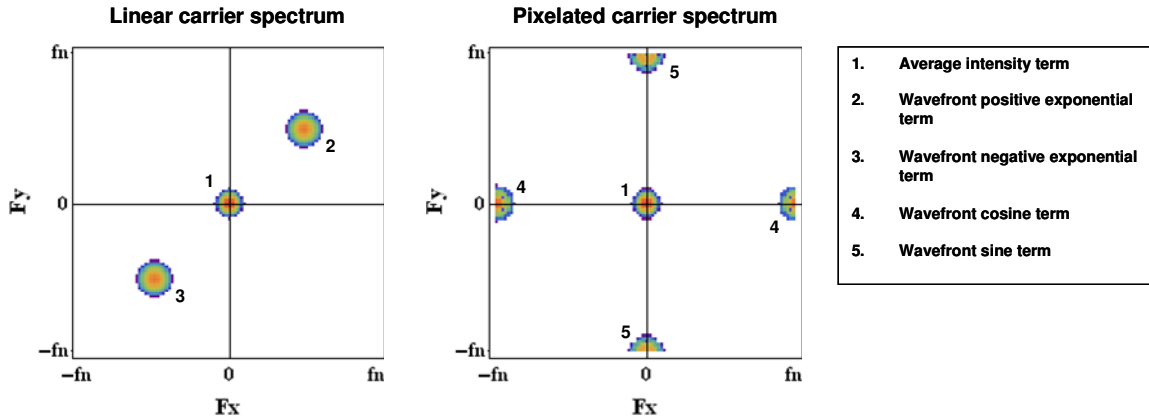


Figure 2. Linear and pixelated carrier interferogram spectral magnitudes. In each case the average intensity term has been broadened for clarity and the maximum wavefront slope is 0.05 waves/pixel.

As is demonstrated in figure 2, adding the spatial carrier phase to the wavefront phase has separated the wavefront terms from the average intensity term in the Fourier domain. There are several different techniques for determining the wavefront phase from the spatial carrier interferogram. In the most general sense they involve suppression of the average intensity term, component 1, and filtering out the two wavefront terms, components 2 and 3 in the spectrums of figure 2. These calculation techniques may be carried out in the spatial domain, the Fourier domain or both.⁴

One technique for determining the wavefront phase from the spatial carrier interferogram is the spatial low pass filtering method. In this technique the spatial carrier interferogram intensity values are first multiplied by the sine and cosine of the carrier phase forming spatial heterodyne wavefronts. These two products are then low-pass filtered by convolution with a filter kernel in the spatial domain to remove the DC and double frequency terms. The demodulated phase is given by the arctangent of the ratio of the filtered sine and cosine products.³ Figure 3 provides an outline of the spatial low-pass filtering process.

Spatial Low Pass Filtering

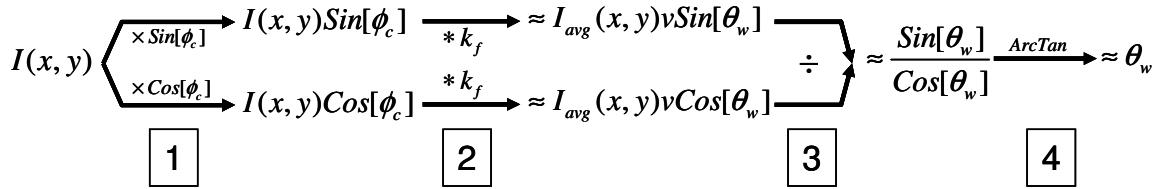


Figure 3. Spatial low pass filtering process steps. 1. Form two heterodyne signals by multiplying the spatial carrier interferogram by the sine and the cosine of the carrier phase. 2. Filter out the DC and double frequency terms in the heterodyne signals by convolving with a filter kernel. 3. Form the ratio of the filtered heterodyne terms. 4. Take the arctangent of the terms ratio to determine the phase.

Although this technique is generally carried out strictly in the spatial domain, we will continue to analyze the steps in the Fourier domain for clarity. The spectral magnitude of the spatial heterodyne signals for the linear and pixelated carriers is shown in Figure 3. In each case the heterodyne signal was formed by multiplying each interferogram with the cosine of the carrier phase.

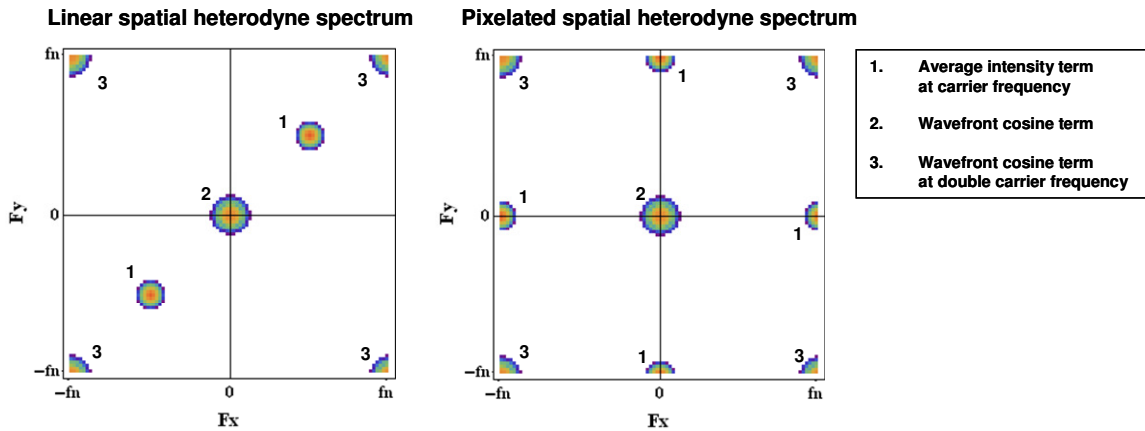


Figure 4. Linear and pixelated carrier spatial heterodyne spectral magnitudes. The heterodyne signal is formed by multiplying the spatial carrier interferogram by the cosine of its carrier phase.

The critical step with regard to the phase resolution of our phase calculation technique involves the low pass filtering of the central wavefront term. Containing the wavefront phase term of interest, the central term, items 2 in figure 3, must be filtered out without significant attenuation. The average intensity terms and the double frequency wavefront terms, items 1 and 3 in figure 3, must be significantly attenuated. If filtered too much, then the phase resolution of the measurement will be degraded. If not filtered enough, then the average intensity terms and the double frequency terms will introduce high frequency noise into the result.⁵ The accuracy of the calculated wavefront phase associated with the detected interferogram is ultimately set by the sharpness of our filter. As wavefront slopes increase, the central wavefront terms will expand and the double frequency terms will alias in toward the center, making the filtering process more difficult. The spectrum of the linear and pixelated heterodyne signals for a wavefront containing large slopes is shown in figure 5.

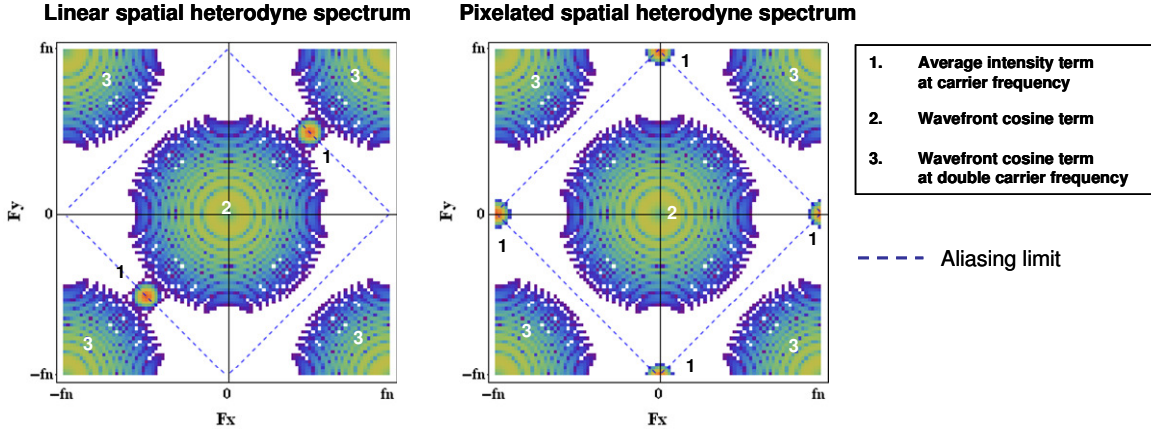


Figure 5. Linear and pixelated carrier spatial heterodyne spectral magnitudes for a wavefront with large slopes. In each case the average intensity term has been broadened for clarity and the maximum wavefront slope is 0.32 waves/pixel. The dashed line indicates the sharp filter limit for a wavefront with only tilt and a flat average intensity.

Referring to figure 5, in both the linear and pixelated cases we are limited to half the Nyquist frequency in directions along the diagonals. Note that this is equal to $\frac{\sqrt{2}}{2}$ times the Nyquist limit along the horizontal or vertical directions. This is because this is the point at which separation of the central term from the average intensity term and the double frequency term in the linear case, or from the double frequency term in the pixelated case, would be impossible. It should be noted, that since the pixelated heterodyne signal places the average intensity term out at the Nyquist limit it is more tolerant than the linear carrier technique to larger variations in the average intensity. If a symmetric filter with a step edge cutoff were possible, the dashed line in each spectrum indicates the maximum spatial frequency to prevent aliasing for a wavefront with only tilt and a flat background intensity.

Low pass filtering of the pixelated heterodyne spectrum is done in the spatial domain through convolution with one of two filter kernels, a 2x2 filter kernel or a 3x3 filter kernel. Both kernels and their associated filter functions are shown in figure 6. A cross sectional plot of the filter functions is also shown.

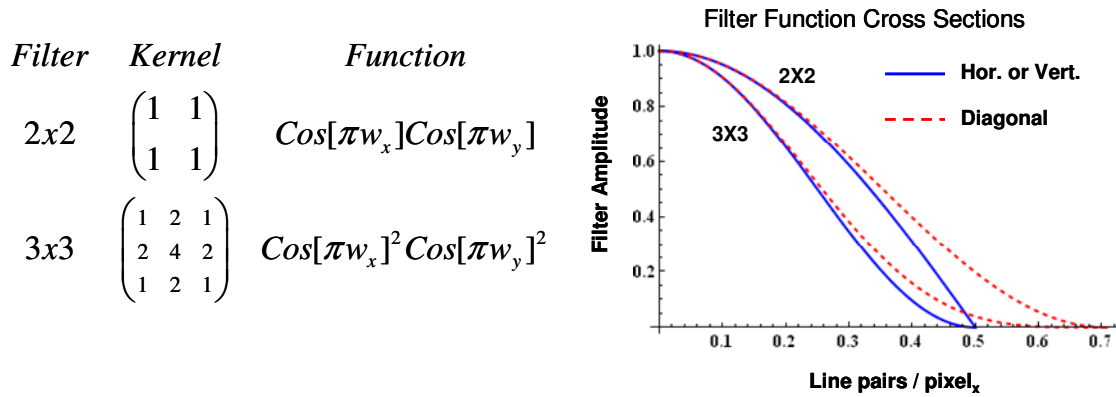


Figure 6. Pixelated mask filter kernels and their associated filter functions.

In figure 7 the pixelated heterodyne spectrum is shown overlaid with contour plots of the two different filter functions.

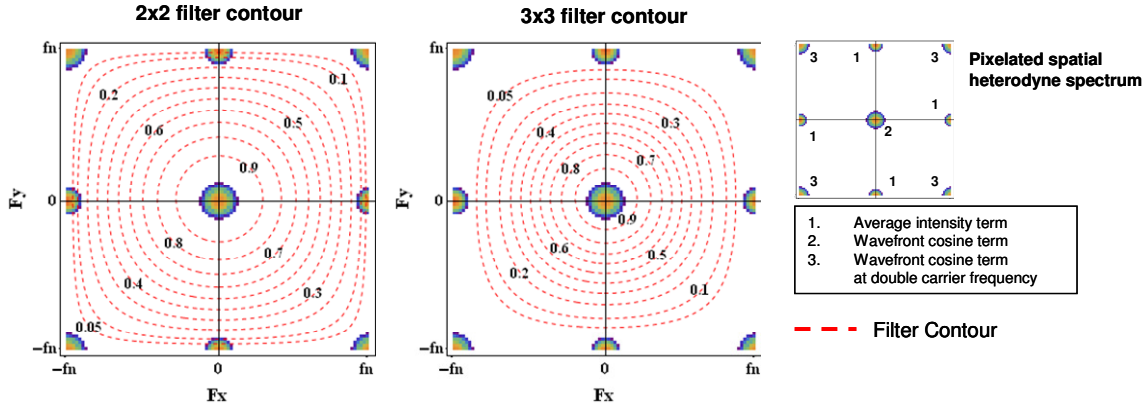


Figure 7. Pixelated spatial heterodyne spectrum with contour overlays of the processing filter functions.

It is obvious from looking at the above filter function plots that the 2x2 kernel has better high frequency performance due to a steeper roll-off. However, note that the 2x2 filter has a very sharp slope at the Nyquist limit, whereas the 3x3 filter has a broader area of attenuation. The filter must remove the DC term from the interferogram at this point. If the illumination is non uniform, then the average intensity term can have a significant spectral width. In this case the 3x3 filter would be a better choice for attenuating this term, preventing it from introducing high frequency noise into the phase calculation.

3. INSTRUMENT TRANFER FUNCTION

The primary factors affecting the ability of an interferometer to accurately determine the phase profile of the object under test are the illumination source spatial and spectral characteristics, the imaging system, the detector sampling, and the phase calculation technique. The basic process of an interferometric measurement for a coherent spatial carrier system is outlined below in figure 8. The process has been separated into three sections; imaging, detection, and computation. Taken by themselves, each of the sub processes is characterized by a linear transfer function. However, due to the non-linearity of the interferometric phase calculation process, the net system transfer function relating the calculated phase spectrum to the object phase spectrum can only be associated with the product of the individual transfer functions under limited conditions. Goodman⁷ provides a rigorous treatment of linear system theory as applied to optics. Additionally, an excellent general discussion concerning an interferometric instrument transfer function is provided by de Groot.⁸

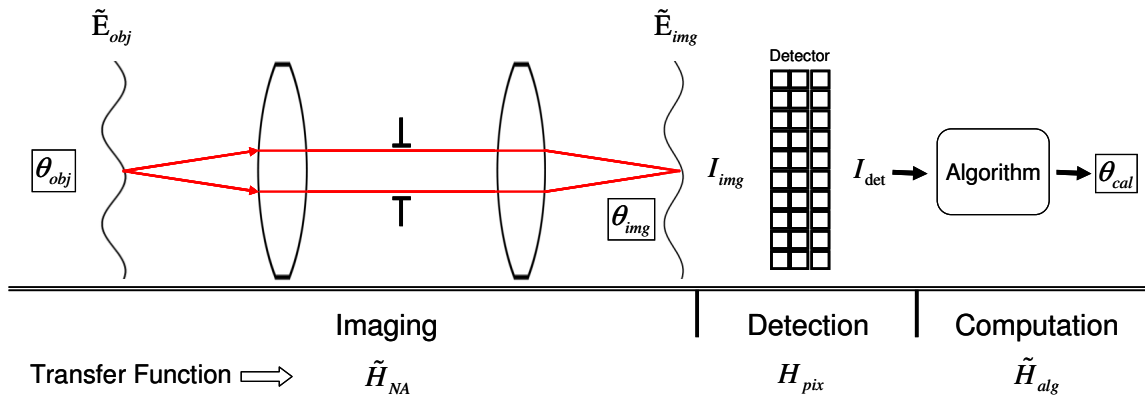


Figure 8. Interferometric measurement process.

For an interferometric system measuring surface height, the instrument transfer function (ITF) is the ratio between the calculated surface height and the actual object surface height as a function of spatial frequency. In general, the instrument transfer function is not independent of the object being measured due to the non-

linear nature of the interferometric process. Since the surface height values are directly proportional to the calculated phase, the ITF may be expressed in terms of wavefront phase as follows:

$$\mathfrak{S}\{\theta_{cal}\} \equiv ITF \mathfrak{S}\{\theta_{obj}\} \quad (8)$$

The first step in the interferometric measurement process is the imaging of the object electric field at the detector plane. Since the system being discussed is strictly coherent, the relationship between the object and image electric fields is given by equation 1.

$$\mathfrak{S}\{E_{img}\} = \tilde{H}_{NA} \mathfrak{S}\{E_{obj}\} \quad (9)$$

where $\mathfrak{S}\{\}$ designates the Fourier transform and \tilde{H}_{NA} is the coherent transfer function. At the detector plane the image test and reference field interfere and are sampled by the detector array. The relationship between the image interferogram and the detected interferogram is shown in equation 10.

$$\mathfrak{S}\{I_{det}\} = H_{pix} \mathfrak{S}\{I_{img}\} \quad (10)$$

where H_{pix} is the detector transfer function associated with the finite pixel size. The final step is the phase calculation process.

As discussed in section 2, the low pass filtering method of spatial carrier interferometry requires filtering the interferogram heterodyne signals to separate out the wavefront component. This process may be represented as follows:

$$\tilde{I}_{HET} \equiv I_{det} e^{i\phi_c} \quad (11)$$

$$\mathfrak{S}\{\tilde{I}_{alg}\} = H_f \mathfrak{S}\{\tilde{I}_{HET}\} \quad (12)$$

$$\theta_{calc} = \text{modulus}[\tilde{I}_{alg}] \quad (13)$$

where \tilde{I}_{HET} is the complex heterodyne signal, H_f is the phase processing algorithm filter function, \tilde{I}_{alg} is the complex filtered heterodyne signal and will be referred to as the algorithm intensity, and θ_{calc} is the calculated phase. Combining equations 11,12, and 13 gives:

$$\mathfrak{S}\{\tilde{I}_{alg}\} = H_f \left(H_{pix} \mathfrak{S}\{I_{img}\} * \mathfrak{S}\{e^{i\phi_c}\} \right) \quad (14)$$

where $*$ represents the convolution operation. The image intensity spectrum is given by the autocorrelation of the electric field spectrum given in equation 9.⁷ This operation is shown below in equation 15.

$$\mathfrak{S}\{I_{img}\} = \left(H_{NA} \mathfrak{S}\{E_{obj}\} \right) \otimes \left(H_{NA} \mathfrak{S}\{E_{obj}\} \right) \quad (15)$$

where \otimes represents the auto correlation operation. Clearly, the relationship between the image and the object intensity spectrums is non-linear. Restricting the test object to surface heights $\ll \lambda/4$ ⁸, equation 15 may be simplified to:

$$\mathfrak{S}\{I_{img}\} \approx H_{NA} \mathfrak{S}\{I_{obj}\} \quad (16)$$

Substituting equation 16 into equation 14 gives:

$$\mathfrak{S}\{\tilde{I}_{alg}\} = H_f \left(H_{pix} H'_{NA} \mathfrak{S}\{I_{obj}\} * \mathfrak{S}\{e^{i\phi_c}\} \right) \quad (17)$$

Substituting the object intensity of equation 1 into equation 17 gives:

$$\mathfrak{S}\{\tilde{I}_{alg}\} = H_{pix} H'_{NA} H_f \left(\mathfrak{S}\{I_{avg} v e^{i\theta_w}\} + \mathfrak{S}\{I_{avg} e^{i\phi_c}\} + \mathfrak{S}\{I_{avg} v e^{i\theta_w + 2\phi_c}\} \right) \quad (18)$$

Assuming that the filtering is sufficient to remove both the single and double frequency carrier terms, and noting that $H'_{NA} H_{pix}$ is simply the system optical transfer function, equation 18 may be reduced to:

$$\mathfrak{S}\{\tilde{I}_{alg}\} = OTF H_f \mathfrak{S}\{I_{avg} v e^{i\theta_w}\} \quad (19)$$

Converting equation 19 to the spatial domain gives:

$$\tilde{I}_{alg} = k_{OTF} * k_f * I_{avg} v e^{i\theta_w} \quad (20)$$

were k_{OTF} and k_f are the filter kernels associated with the OTF and H_f respectively, and $*$ represents the convolution operation. Assuming the variance of the average intensity term is low, it is taken outside the convolution operation.

$$\tilde{I}_{alg} = I_{avg} v (k_{OTF} * k_f * e^{i\theta_w}) \quad (21)$$

Using the previous assumption of small wavefront deviation the exponential term of equation 21 is expanded through the first order.

$$k_{OTF} * k_f * e^{i\theta_w} \simeq k_{OTF} * k_f * (1 + i\theta_w) = 1 + i(k_{OTF} * k_f * \theta_w) \simeq e^{i(k_{OTF} * k_f * \theta_w)} \quad (22)$$

where it was assumed that the filter kernels are normalized. Using this result, equation 21 may be written as:

$$\tilde{I}_{alg} = I_{avg} v e^{i(k_{OTF} * k_f * \theta_w)} \quad (23)$$

Finally, substituting equation 23 into equation 13, the calculated phase is given in both the spatial and Fourier domain as:

$$\theta_{calc} \simeq k_{OTF} * k_f * \theta_w \quad (24)$$

$$\mathfrak{S}\{\theta_{calc}\} \simeq OTF H_f \mathfrak{S}\{\theta_w\}$$

A comparison of equations 8 and 24 gives the final result for the instrument transfer function of a spatial carrier interferometer for wavefronts with small phase deviations:

$$ITF \simeq OTF H_f \quad (25)$$

where once again, H_f is the spatial carrier filter transfer function given in figures 6 and 7.

In summary, with the assumption of small surface deviations, $\ll \lambda/4$, the instrument transfer function, ITF, of a spatial carrier interferometer may be approximated by the product of the system OTF and the spatial carrier processing filter, H_f . Additionally, just as the detector pixel spacing defines a spatial frequency limit, the Nyquist frequency, necessary to prevent aliasing of high frequency information; the carrier

frequency also defines a maximum spatial frequency limit necessary to prevent the aliasing of high frequency heterodyne components into the measured phase.

4. SIMULATED SURFACE WITH A FLAT POWER SPECTRUM

An easy way to determine the affects of the pixelated mask sensor on the ITF is to simulate a measurement on a surface with a flat power spectrum. A 1000 x 1000 array of uniformly distributed random numbers was generated for the surface. The distribution had a mean of zero and an RMS of 0.1 waves. For this simulation the OTF was assumed to be equal to 1 for all frequencies out to Nyquist. The surface phase was then added to the pixelated mask phase and a simulated interferogram was generated. Next, phase calculations were conducted using the 2x2 and the 3x3 algorithms. Finally, the PSD for the calculated phase was determined. In this case, since the initial PSD was flat, the ITF is simply the square root of the calculated PSD with the necessary normalization applied. In order to reduce noise, the final ITF curves are the average of 100 simulations. Both measured, dashed lines, and theoretical, solid lines, are shown in figure 9. The theoretical curves are the filter functions given in figure 6. With the exception of the noise due the random surface generation, the simulated and theoretical curves are in agreement.

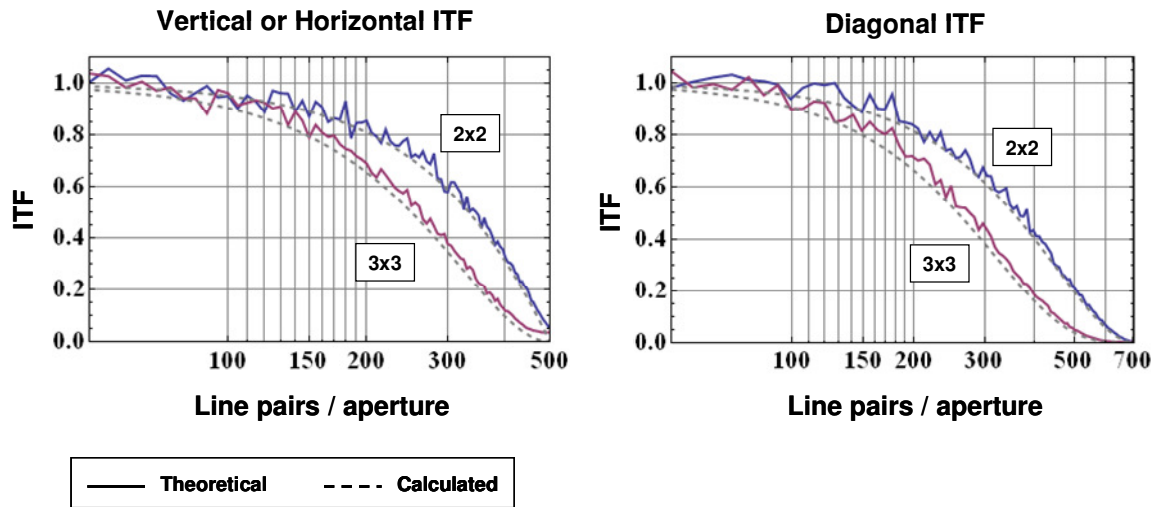


Fig. 9. Measured ITF of a simulated surface with a flat power spectrum using the 2x2, and 3x3 pixelated algorithms. The dashed lines indicate the calculated ITF while the solid curves are the theoretical values.

5. MODELING A STEP RESPONSE

In order to determine the effect of the pixelated mask sensor and associated algorithms on the ITF, a simulated step height measurement was performed. The simulation assumed a step height of 0.2 waves oriented along the y-axis. The imaging was strictly coherent with the system numerical aperture set to produce a cutoff frequency of $\frac{1}{2}$ wave per pixel at the camera. The system was assumed to be diffraction limited. The camera sensor was simulated by an array of 1000 x 1000 pixels with 100% fill factor (i.e. there are no gaps between the pixels). The ITF curves shown in Figure 10 were determined by the following procedure:

1. Generate an electric field associated with a 0.2 wave step height, and a flat reference surface. Oversample field by a factor of 10 compared with the CCD pixel sampling.
2. Propagate the electric field from the object and reference to the pixelated mask.
3. Add pixelated mask phase offset to object and reference electric fields. Skip this step for calculating the temporal phase shift ITF curve.
4. Calculate the intensity at the CCD by summing the electric fields and then squaring.
5. Convolve the intensity with a square pixel and then sample the result at the pixel spacing.

6. Calculate the phase using the 2x2 parsed algorithm, the 2x2 convolution algorithm, the 3x3 convolution algorithm and a simple 4 step temporal algorithm.
7. Determine the power spectral density (PSD) for each phase calculation
8. Normalize each PSD by the PSD of a perfect step.
9. Take the square root of the normalized PSDs to obtain the ITFs.

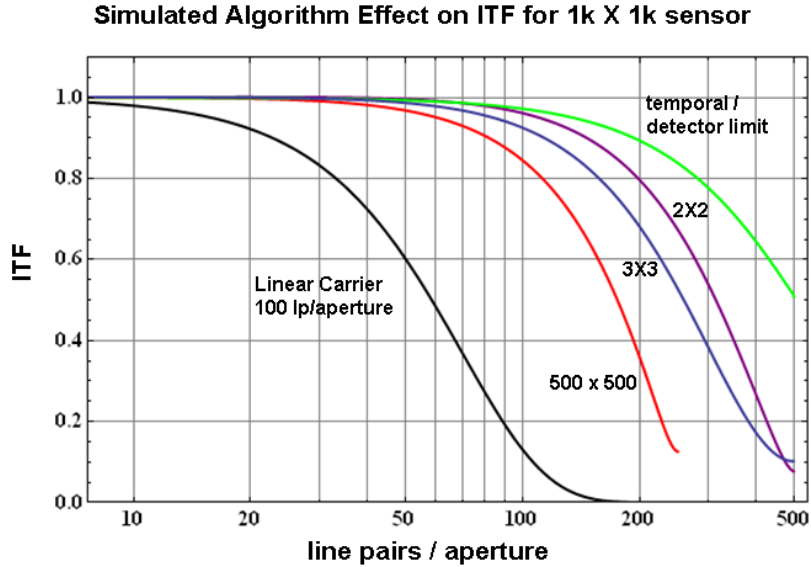


Fig. 10. Instrument transfer function calculated for the pixelated mask sensor and associated algorithms. The calculation is based on a simulated 0.2 wave step measurement. The camera sensor is a 1000 x 1000 array of square pixels. The ITF of a temporal measurement, which is shown for comparison, is the limit due to the pixel width. The 500 x 500 trace represents the temporal ITF that would be obtained by an array with pixels twice as wide (i.e. 1/4 the number of pixels). The 2X2 and 3X3 traces show the response of the convolution method for the respective kernel sizes. The Linear Carrier trace shows the effective resolution of a Fourier Transform method utilizing 100 fringes of tilt as the carrier and a Gaussian filter.

These calculations show that using the convolution technique with the pixelated sensor preserves a significant portion of the spatial frequency spectrum. In this example for a 1000 x 1000 array, the curve labeled “temporal” is the maximum resolution that can be achieved, assuming a diffraction limited optical system and pixels with 100% fill factor. The curve labeled “500x500” represents the frequency response that would be achieved for an array with 1/4 the number of pixels that are twice as wide (equal to 4 pixels of the 1000x1000 sensor). For the pixelated phase sensor, the 500x500 curve represents the resolution that would be achieved if the array was sub-divided into unique groups of 4 neighboring pixels, and a single phase value was calculated for each sub-group. Utilizing the convolution algorithm extends the frequency response out to the limit of the full sensor resolution, significantly beyond the 500 x 500 limit. Also shown for comparison in Figure 9 is the response of a phase measurement utilizing the spatial carrier method. 100 fringes of linear tilt are used to generate the carrier frequency on a 1000x1000 sensor. In this case, the ITF is significantly limited by the frequency response of the spatial carrier processing filter.

6. FIZCAM 2000 STEP HEIGHT MEASUREMENT ITF CALCULATION

In order to verify the results of the simulation in section three, the ITF of a FizCam2000 was determined by measuring a 0.2 wave step height standard.⁹ The imaging in the FizCam2000 is strictly coherent. The step standard is formed on a 1 inch optical flat and has uniform reflectivity on each side of the step. As in the simulation above, the step was oriented along the y-axis. The calculated ITF along with the corresponding simulated ITF curve is shown below in figure 11. These measurements confirm that the instrument ITF follows the theoretical response.

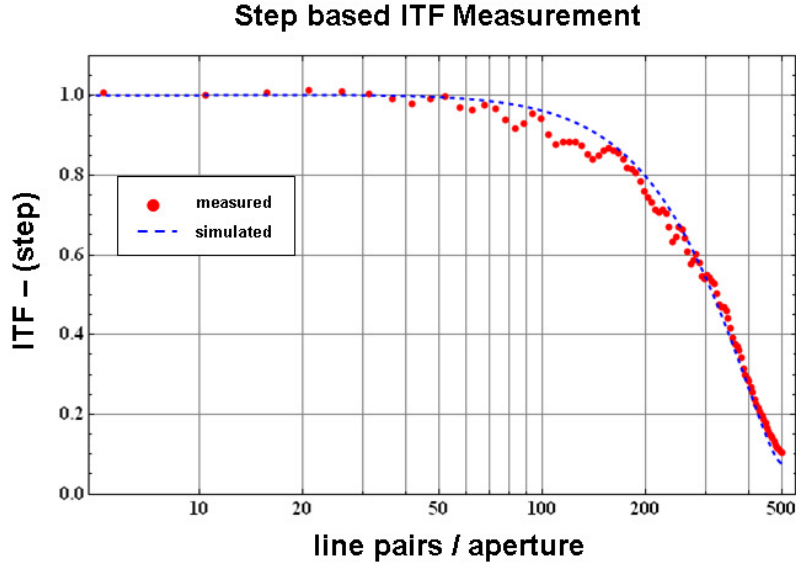


Fig. 11. Measured instrument transfer function (ITF) for the Fizzcam 2000 using the 2x2 algorithm. The calculation is based on a 0.2 step height measurement. The system aperture size is 100mm. The theoretical ITF of the 2x2 is shown as the dotted line.

7. SMOOTH SURFACE MEASUREMENT

An additional check on the transfer function characteristic of the pixelated sensor was conducted by measuring a relatively smooth glass surface, < 0.5 nm RMS. The left graph in figure 12 shows the horizontal or vertical PSD curves. The right graph provides the corresponding curves for the diagonal, 45 deg., PSD. In each case the theoretical curves for the 2x2 and 3x3 algorithms are given as dashed gray lines. The theoretical curves were generated by fitting the linear portion of the measured PSD curves and then modifying the curve to take into account the sample spacing and the filter transfer function. For the diagonal PSD curves, significant departure from the theoretical curves occurs at higher spatial frequencies due to aliasing with the double frequency heterodyne terms as discussed in section 4. Additional aliasing occurs in the sub sampled curve due to the down sampling affect.

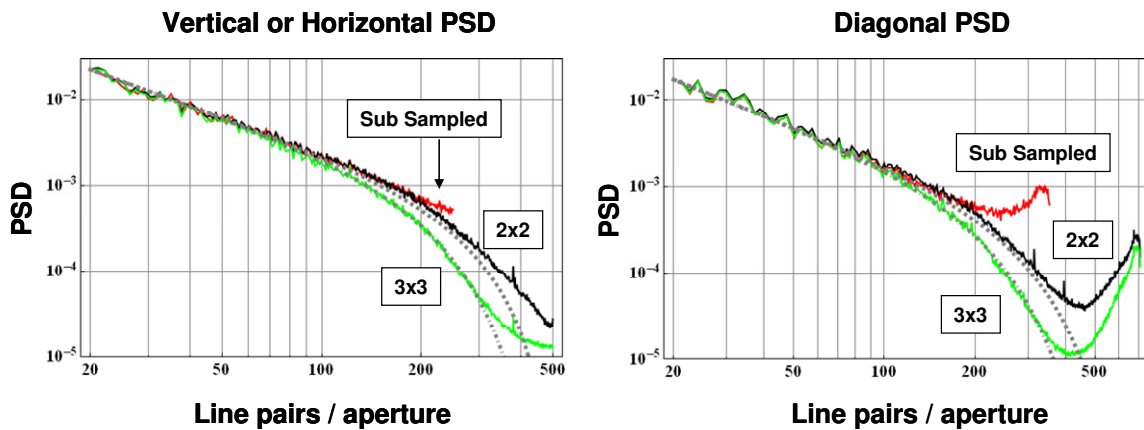


Fig. 12. Measured PSD of a smooth glass surface using the 2x2, 3x3, and sub sampled 2x2 algorithms. The dashed gray lines indicate the theoretical PSD curves for the 2x2, and 3x3 algorithms.

8. CONCLUSIONS

The spatial frequency response of the pixelated phase mask sensor has been investigated both theoretically and experimentally. It was shown that with the assumption of small surface deviations, $\ll \lambda/4$, the instrument transfer function, ITF, of a spatial carrier interferometer may be approximated by the product of the system optical transfer function, OTF, and the spatial carrier processing filter, H_f . Additionally, just as the detector pixel spacing defines a spatial frequency limit, the Nyquist frequency, necessary to prevent aliasing of high frequency information; the carrier frequency also defines a maximum spatial frequency limit necessary to prevent the aliasing of high frequency heterodyne components into the measured phase. The pixelated mask spatial carrier operates at the maximum carrier frequency possible for a given detector. This allows non-aliased measurements on wavefronts with spatial frequency components up to $\sqrt{2}/2$ times the Nyquist sampling limit at its most restrictive.

Actual measurements on a production Fizeau interferometer agree very well with the theory, and demonstrate detector limited performance. The spatial resolution of the calculated phase map is algorithm dependent; however, both the 2x2 and 3x3 convolution algorithms result in a frequency response that is significantly more than what would be obtained by a simple parsing of the image into 4 pixel cells and, with some attenuation, extends to the full Nyquist limit of the sensor along the x and y axis.

REFERENCES

1. J. E. Millerd, N. J. Brock, J. B. Hayes, M. B. North-Morris, M. Novak, and J. C. Wyant, "Pixelated phase-mask dynamic interferometer," Proc. SPIE 5531, 304-314, (2004).
2. J. E. Millerd in "Fringe 2005," edited by W. Osten, (Springer, New York, 2005), pg 640.
3. B. Kimbrough, J. Millerd, J. Wyant, J. Hayes, "Low Coherence Vibration Insensitive Fizeau Interferometer," Proc. SPIE 6292, (2006).
4. D. Malacara, M. Servin, and Z. Malacara, "Interferogram analysis for optical testing," (Marcel Dekker, New York, 1998).
5. Womack, K. H. "Interferometric phase measurement using spatial synchronous detection." Optical Engineering, 23(4): 391-395, 1984
6. Kimbrough, B. "Pixelated mask spatial carrier phase shifting interferometry-algorithms and associated errors." Appl. Opt. 45, 4554-4562, 2006
7. Goodman, "Introduction to Fourier Optics", McGraw-Hill, 1996
8. Peter de Groot, Xavier Colonna de Lega, "Interpreting Interferometric height measurements using the instrument transfer function," in "Fringe 2005," edited by W. Osten, (Springer, New York, 2005)
9. E. Novak et al., "Optical resolution of phase measurements of laser Fizeau interferometers," Proc. SPIE 3134, 114-121 (1997)